Imaging of lung cancer with fluorine-18 fluorodeoxyglucose: comparison of a dual-head gamma camera in coincidence mode with a full-ring positron emission tomography system

W.A. Weber[1], J. Neverve[1], J. Sklarek[4], S.I. Ziegler[1], P. Bartenstein[1], B. King[4], T. Treumann[3], A. Enterrottacher[1], M. Krapf[1], K.E. Häußinger[6], H. Lichte[7], H.W. Präuer[2], O. Thetter[4], M. Schwaiger[1]

[1] Department of Nuclear Medicine, Technische Universität München, Germany
[2] Department of Surgery[2], Technische Universität München, Germany
[3] Department of Radiology, Technische Universität München, Germany
[4] Department of Surgery, Fachklinik München-Gauting, Germany
[5] Department of Radiology, Fachklinik München-Gauting, Germany
[6] Department of Internal Medicine, Fachklinik München-Gauting, Germany
[7] Department of Nuclear Medicine, Fachklinik München-Gauting, Germany

Received 29 August and in revised form 7 December 1998

Abstract. Dual-head gamma cameras operated in coincidence mode are a new approach for tumour imaging using fluorine-18 fluorodeoxyglucose (FDG). The aim of this study was to assess the diagnostic accuracy of such a camera system in comparison with a full-ring positron emission tomography (PET) system in patients with lung cancer. Twenty-seven patients (1 female, 26 males, age 62±9 years) with lung cancer or indeterminate pulmonary nodules were studied on the same day with a full-ring PET scanner (Siemens ECAT EXACT) and a coincidence gamma camera system (ADAC Vertex MCD). Sixty minutes after injection of 185–370 MBq FDG, a scan of the chest was performed with the full-ring system. Approximately 2 h p.i., the coincidence camera study was performed. Coincidence gamma camera (CGC) and PET images with (PETac) and without attenuation correction (PETnac) were analysed independently by two blinded observers. In addition, FDG uptake in primary tumours and involved lymph nodes was quantified relative to normal contralateral lung (T/L ratios). All primary tumours were histologically proven. The lymph node status was histologically determined in 23 patients. In four patients, no lymph node sampling was performed because of extensive disease or concurrent illnesses. In the 27 patients, 25 primary lung cancers and two metastatic lesions were histologically diagnosed. The number of coincidences per centimetre axial field of view was $3.33\pm0.93\times10^5$ for the CGC and $1.09\pm0.36\times10^6$ for the dedicated PET system. All primary tumours (size: 4.6±2.6 cm) were correctly identified in the CGC and dedicated PET studies. T/L ratios were 4.7±2.5 for CGC and 6.9±2.8 for PETnac (P <0.001). Histopathological evaluation revealed lymph node metastases in 11 of 88 sampled lymph node stations (size: 2.3±1.0 cm). All lymph node metastases were identified in the PETac studies, while PETnac detected 10/11 and CGC 8/11. For positive lymph nodes that were visible in CGC and PETnac studies, T/L ratios were 3.7±2.3 for CGC and 6.6±3.1 for PETnac (P=0.02). The diameters of false-negative lymph nodes in the CGC studies were 0.75, 1.5 and 2 cm. False-positive FDG uptake in lymph nodes was found in two patients with all three imaging methods. For all lesions combined, T/L ratios in CGC relative to PETnac studies decreased significantly with decreasing lesion size (r=0.62; P<0.001). In conclusion, compared with a full-ring PET system the sensitivity of CGC imaging for detection of lung cancer is limited by a lower image contrast which deteriorates with decreasing lesion size. Nevertheless, the ability of CGC imaging to detect pulmonary lesions with a diameter of at least 2 cm appears to be similar to that of a full-ring system. Both systems provide a similar specificity for the evaluation of lymph node involvement.

Key words: Positron emission tomography – Dual-detector coincidence imaging – Fluorodeoxyglucose – Lung cancer

Eur J Nucl Med (1999) 26:388–395

Correspondence to: W.A. Weber, Nuklearmedizinische Klinik, Klinikum Rechts der Isar, Ismaningerstrasse 22, D-81675 München, Germany

Introduction

The potential value of positron emission tomography (PET) using the glucose analogue fluorine-18 fluorode-

oxyglucose (FDG) for the imaging of malignant tumours has been widely documented in the literature [1]. In particular, numerous studies in recent years have demonstrated that FDG-PET is the most accurate non-invasive method for the detection and staging of lung cancer [2–8]. This is attributable to the fact that lung cancer cells show high uptake of FDG while the background activity in normal lung and mediastinum is low.

These encouraging results have attracted considerable clinical interest in imaging lung cancer with FDG. However, the high cost of FDG-PET studies has prevented widespread application of this technique. Generally, ring detector systems with bismuth germanate (BGO) crystals are used for FDG studies in cancer patients. These systems are considerably more expensive than conventional gamma cameras and are exclusively applicable for imaging with positron-labelled compounds.

In 1996, a modification of a dual-detector single-photon emission tomography (SPET) system to enable operation in coincidence mode was introduced by Muehllehner and colleagues. This system is capable of operating in coincidence mode as well as imaging lower energy photons, such as the 140 keV photons of technetium-99m. The evaluation of the performance characteristics of these systems according to NEMA standards yielded encouraging results. The volume sensitivity and spatial resolution were found to be comparable to those of a dedicated ring system operated in 2D mode [9]. An initial clinical study [10] showed promising results for the evaluation of pulmonary lesions: 13 of 14 intrapulmonary lesions visualized by a dedicated ring system were detected by the coincidence gamma camera [10].

In the present study, we evaluated the diagnostic accuracy of coincidence gamma camera imaging for the detection of lung cancer and mediastinal staging using histopathological diagnosis as the gold standard. Diagnostic results were compared with those obtained using a full-ring PET scanner and computed tomography. Furthermore, count rates and image contrast were determined for the coincidence camera and compared with the results for a full-ring PET system.

Materials and methods

A total of 27 patients (1 female, 26 males, age 62±9 years) were included in the study. Twenty-five patients had clinically suspected or biopsy-proven non-small-cell lung cancer. Two patients were studied for the evaluation of indeterminate pulmonary nodules. All patients were imaged on the same day with a full-ring PET system (CTI/Siemens ECAT EXACT 47) and a dual-detector gamma camera operated in coincidence mode (Vertex, Molecular Coincidence Detection, ADAC Laboratories). After a single injection of FDG, the patients were studied first with the full-ring system followed by the coincidence gamma camera. Computed tomography (CT) of the chest was performed as part of the routine staging within 2 weeks of the FDG studies (spiral CT in 17 cases, conventional CT in ten cases). Patients fasted for at least 4 h prior to PET imaging in order to minimize glucose utilization of normal tissue and to ensure standardized glucose metabolism in all patients. Details of the study were explained to the patients by a physician and written informed consent was obtained. The study protocol was reviewed and approved by the Ethics Committee of the Technische Universität München.

Fluorine-18 was produced with a self-shielded 11-MeV cyclotron (RDS 112; Siemens/CTI) by the acceleration of protons onto an oxygen-18 water target. FDG was synthesized using a standard technique modified from the synthesis reported by Hamacher et al. [11].

Imaging with full-ring PET system

The ECAT EXACT PET scanner consists of 24 rings of BGO detectors that yield 47 transverse slices, 3.4 mm apart [axial field of view (FOV): 16.2 cm]. According to NEMA standards, the spatial resolution in axial and transaxial directions is 5 and 5.8 mm, respectively [12]. Sixty minutes after injection of 185–370 MBq FDG (mean: 214±49 MBq) a single static emission scan of 20 min duration was acquired in 2D mode. The FOV included the chest from the thoracic inlet to below the carina. After the emission scan, a 15-min transmission scan for attenuation correction was performed. This scan yielded approximately 1.5×10^6 counts/slice. Images were reconstructed with and without attenuation correction using a penalized least square algorithm developed by Fessler [13].

Imaging with coincidence gamma camera (CGC)

The Vertex MCD camera is a dual-head gamma camera equipped with 5/8″ sodium iodide (NaI) crystals which are placed into coincidence mode. Patients were imaged over the entire thorax and upper abdomen (one bed position in ten patients, two bed positions in 17 patients). The axial FOV was 38 cm when one bed position was used and 57 cm when two bed positions were employed. Prior to image acquisition, the singles count rate was determined on the rate meter of the camera. Imaging was started when the singles rate was below 1.5×10^6/s. The interval between FDG injection and start of the image acquisition was 126±27 min. All patients were imaged for 32 stops through a rotation of 180° per detector at 40 s/frame for a total acquisition time of approximately 23 min per bed position. Data were acquired in 3D mode and decay correction was performed during the acquisition. Images were not corrected for photon attenuation. The energy windows were set at 511 keV/30% for the ^{18}F photopeak and 310 keV/30% for the Compton events in the NaI crystal. The coincidence mode of acquisition utilized all photopeak-photopeak events as well as the photopeak-Compton scatter events. No Compton-Compton coincidences were accepted. The detectors provide a timing resolution of 6 ns and a 15-ns timing window was used to acquire the coincidence events. According to NEMA standards the resolution in axial and transaxial direction (full-width at half-maximum, FWHM) is approximately 5 mm [9].

Each data set was rebinned utilizing single slice rebinning and reconstructed using an ordered subset expectation maximization (OSEM) iterative algorithm [14]. The parameters used to perform the iterative reconstruction included an ordered subset of 8 with a Wiener pre-filter and a noise factor of 0.7 with 2 iterations.

Surgical staging

Histological diagnoses of all primary lesions were obtained by biopsy (n=3) or thoracotomy (n=24). Mediastinal lymph nodes

were evaluated in 22 patients (thoracotomy in 21 cases, mediastinoscopy in one case). In these patients, 88 lymph node stations according to the AJCC (American Joint Committee on Cancer) classification [15] were sampled and histopathologically examined. Only lymph nodes in the areas 10 and 11 were considered to be N1 or hilar nodes. Peritumoural lymph nodes were not included in the analysis because it is often not possible to differentiate these nodes from the primary tumour in CT or PET studies.

Data analysis

Visual interpretation. For comparison of the CGC and the full-ring PET, three sets of images were read separately by two blinded observers (P.B. and W.A.W):

1. CGC images
2. Full-ring PET system without attenuation correction (PETnac)
3. Full-ring PET with attenuation correction (PETac)

Images were interpreted on the computer screen using a linear grey scale. All lesions presenting with focally increased FDG uptake within the mediastinum and the lung were reported as abnormal. The location of lesions was described as intrapulmonary, hilar or mediastinal. For further analysis, a consensus interpretation regarding the presence and location of lymph node metastases was obtained in all cases.

CT scans of the chest were analysed by two blinded radiologists (B.K. and T.T.). A lymph node station was considered as positive when a lymph node with a short-axis diameter of more than 1.0 cm was identified [16–18].

Quantitative analysis. The singles and coincidence count rate at the beginning of the CGC studies were determined from the rate meter of the camera system. The total number of coincidence events recorded during the CGC and dedicated PET studies was determined from the raw data files. For better comparison of CGC and PET studies, the total coincidence counts were divided by the width of the axial FOV.

Circular regions of interest (ROIs) with a diameter of 2 cm were placed over all primary tumours using the plane with the maximum FDG uptake. For quantitative analysis of FDG uptake in lymph node metastases, a circular ROI with a diameter of 1.5 cm was used. A large, irregular ROI in the contralateral lung was chosen as a reference region. Image contrast was expressed as a ratio between the mean counts in the tumour and the reference ROI (T/L ratio). In the PETac studies, the mean standardized uptake value normalized to injected dose and body weight (SUV) was determined for all lesions [19].

Table 1. Characteristics of the study patients

Patient no.	Age (years)	Sex	Tumour type	Lesion size (cm)	pT stage	SUV	T/L CGC	T/L PETnac	pN (stage)
1	54	m	SCLC	3.5	x	4.7	3.8	5.1	3
2	70	m	Squamous	8.5	3	14.4	11.4	12.6	0
3	75	m	Squamous	8.2	2	4.1	7.9	7.6	0
4	69	m	Squamous	5.0	x	5.9	3.4	4.6	x
5	57	m	Squamous	9.8	4	15.8	6.7	11.6	2
6	53	m	Neuroendocrine	2.7	2	5.6	4.7	6.4	1
7	47	m	Squamous	6.6	4	10.3	5.5	7.3	2
8	43	m	Squamous	3.3	3	7.7	5.5	8.3	1
9	58	m	Squamous	4.0	2	5.0	3.2	5.5	1
10	61	m	Squamous	3.0	1	4.5	2.7	6.4	0
11	72	m	Adenoca.	5.5	2	8.6	5.1	11.6	1
12	69	m	Adenoca.	3.5	2	3.3	2.0	2.9	0
13	56	m	Squamous	2.0	2	10.1	4.9	10.0	1
14	51	f	Large cell	2.0	2	7.5	4.4	9.4	2
15	61	m	Undiff.	5.0	4	10.0	1.5	3.5	0
16	59	m	Squamous	2.5	2	7.7	4.9	7.2	0
17	61	m	Undiff.	9.5	4	7.0	4.8	6.5	x
18	67	m	Squamous	5.8	3	10.1	8.2	8.9	1
19	63	m	Large cell	3.5	x	3.5	5.5	6.7	x
20	66	m	Squamous	5.0	4	8.6	9.6	10.9	x
21	74	m	Squamous	3.5	2	4.9	4.1	7.5	0
22	50	m	Squamous	5.5	3	5.6	4.8	5.9	1
23	63	m	Adenoca.	3.2	3	4.0	1.8	3.5	2
24	76	m	Squamous	9.0	3	7.9	5.4	5.0	2
25	69	m	Squamous	1.5	1	3.7	2.5	4.6	0
26	65	m	Metastasis	0.9	–	2.7	1.3	2.9	–
27	60	m	Metastasis	1.0	–	3.6	1.3	4.0	–

SCLC, Small cell lung cancer; squamous, squamous cell carcinoma; adenoca., adenocarcinoma; large cell, large cell carcinoma; undiff., undifferentiated carcinoma; metastasis, metastatic tumour. pT stage, histopathological tumour stage. SUV, standardized uptake value determined from the attenuation-corrected dedicated PET study T/L CGC, Tumour/lung ratio in the coincidence gamma camera studies. T/L PETnac, Tumor/Lung ratio in the non-attenuation-corrected dedicated PET studies. pN stage histopathological lymph node status

Statistical analysis

Image contrast and count rates in PETnac and CGC images were analysed by linear regression analysis and a paired two-sided *t* test. All statistical tests were performed at the 5% level of significance.

Results

Histopathological evaluation

In the 27 patients 25 primary lung cancers and two metastatic lesions were histologically diagnosed (primary lung cancers: 16 squamous cell carcinomas, three adenocarcinomas, two large cell carcinomas, two undifferentiated carcinomas, one small cell carcinoma and one neuroendocrine carcinoma; metastatic lesions: renal cell carcinoma and rectal carcinoma). Resection of the tumour and determination of the maximum tumour diameter by a pathologist was performed in 23 patients. Four patients did not undergo surgery because of distant or contralateral mediastinal metastases or poor general medical condition. In these patients, the histopathological diagnosis was obtained by biopsy and the maximum tumour diameter was determined in the CT scan.

The mean tumour diameter was 4.6±2.6 cm (range 0.9–9.8 cm). The histopathological tumour stage of the primary lung cancers was T1 in two patients, T2 in nine, T3 in six and T4 in five. The lymph node status was N0 in eight, N1 in seven, N2 in five and N3 in one. In six patients, no mediastinal lymph node sampling was performed due to advanced T4 tumour stage (three patients), metastatic lesions (two patients) or poor general medical condition (one patient). Lymph node metastases were found in seven mediastinal and four hilar lymph node stations. Ten of the 11 positive lymph nodes were enlarged on the CT scan, with a short-axis diameter of more than 1 cm. One lymph node metastasis was found in a normal-sized lymph node (0.75 cm). Involvement of peritumoural lymph nodes was detected in four patients. Table 1 summarizes patient characteristics and tumour stages.

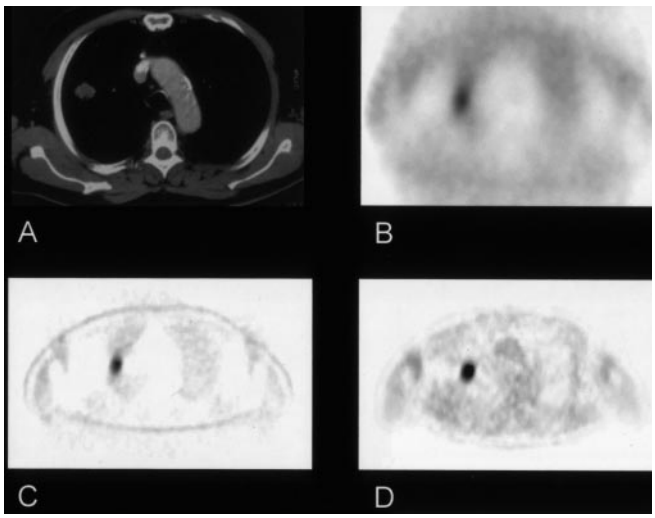

Fig. 1. CT (**A**) CGC (**B**), PETnac (**C**) and PETac (**D**) studies of a patient with a squamous cell carcinoma (patient 16). The tumour shows markedly increased FDG uptake that is clearly visualized on the CGC, PETnac and PETac images. However, background activity is considerably higher on the CGC images than on the PET images

Results of CGC and dedicated PET imaging

Qualitative image interpretation. All intrapulmonary tumours were correctly identified by both observers in the CGC, PETnac and PETac studies. Figure 1 shows an example of a squamous cell carcinoma imaged by CT, CGC, PETnac and PETac. The main difference between CGC and PETnac studies is a considerably higher background activity in the CGC studies. This high background results in blurring of tumour contours and normal anatomical structures.

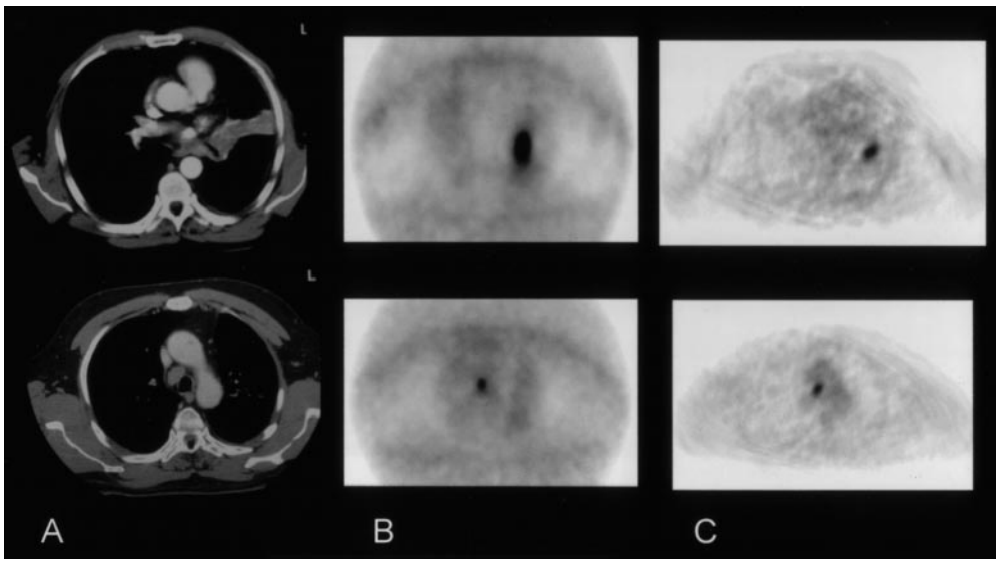

Fig. 2. CT (**A**), CGC (**B**), and PETac (**C**) studies of a patient with small cell carcinoma and mediastinal lymph node involvement (patient 1; *first row*, primary tumour, *second row*, lymph node metastases). CT, CGC and PETac demonstrate increased FDG uptake in the enlarged mediastinal lymph node. Atelectatic lung tissue visualized on the CT image shows no increased FDG uptake

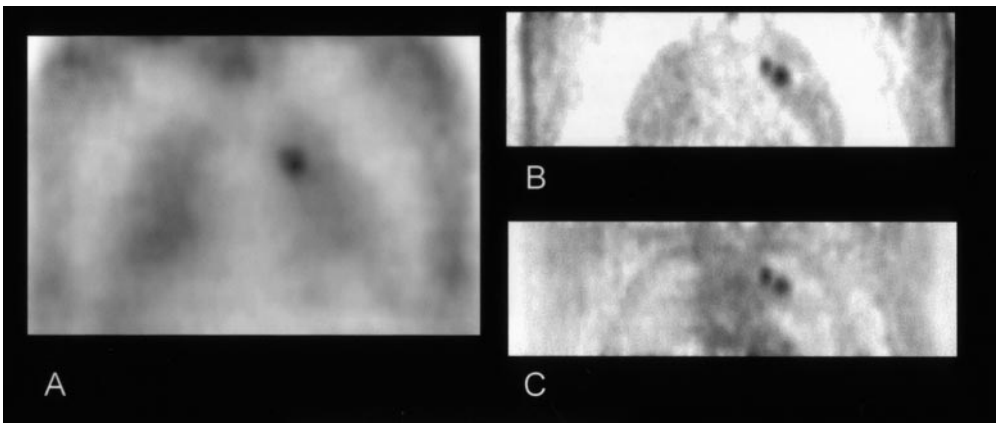

Fig. 3. CGC (**A**), PETnac (**B**), and PETac (**C**) studies of a patient with squamous cell carcinoma (patient 23). The ipsilateral mediastinal lymph node involvement is clearly visible in the PETnac and PETac studies. In the CGC study, the lymph node metastasis cannot be separated from the primary tumour

The 11 histologically confirmed lymph node metastases were correctly identified by CGC, PETnac and PETac in 8, 10 and 11 cases, respectively (Fig. 2). The three false-negatives on CGC were a subcarinal lymph node with a diameter of 0.75 cm, a para-aortic lymph node with a diameter of 1.5 cm and a subcarinal lymph node with a diameter of 2 cm. The two false-negative lymph nodes with diameters of more than 1 cm were located close to the primary tumour. Probably the primary tumour and the lymph node metastasis appeared as one lesion on the CGC images (Fig. 3). The small subcarinal lymph node was also false negative in PETnac. False positive findings occurred in two patients with all imaging techniques. In both cases, non-specific inflammatory changes were detected histologically. PETac and PETnac detected two additional mediastinal lesions that were not surgically sampled because of locally advanced, T4 tumour stage. However, only histologically proven lymph node stations were included in the further analysis. CT detected 10 of the 11 lymph node metastases. In six patients, CT showed enlarged lymph nodes that were histologically negative for tumour. CGC, PETnac and PETac studies were true-negative in four of these patients and also false-positive in two.

Quantitative analysis. At the beginning of the CGC scan, the number of single events was $1.1\pm0.27\times10^6$/s, and the coincidence count rate was $1.4\pm0.4\times10^4$/s. The total number of coincidences recorded per centimetre axial FOV and used for further processing was $3.33\pm0.93\times10^5$/cm for CGC and $1.09\pm0.36\times10^6$/cm for the dedicated PET system ($P<0.001$). The total number of true coincidences, randoms and multiples for the dedicated system was $1.24\pm0.43\times10^6$/cm axial FOV.

The SUV of the pulmonary lesions was 6.9±3.3. The T/L ratio was 4.7±2.5 (median: 4.8) in the CGC studies and 6.9±2.8 (median: 6.5) in the PETnac images ($P<0.001$, Fig. 4). Thus, for the pulmonary lesions the image contrast was 32% lower in the CGC than in the PETnac studies. All pulmonary lesions with a diameter of more than 2 cm had a T/L ratio of at least 1.5 in the CGC studies (mean 5.1±2.4). The SUV of the lymph node metastases was 6.6±3.5 (range: 2.8–12.8). For

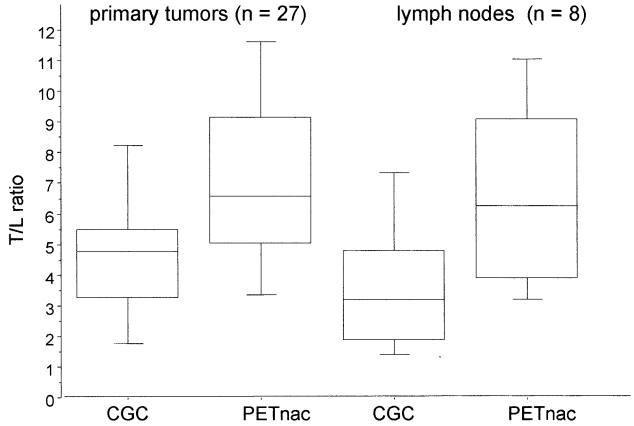

Fig. 4. Tumour/lung ratios (T/L) for primary tumours and lymph node metastases in the CGC and PETnac studies. The *horizontal lines* in this "box plot" represent the 10th, 25th, 50th (median), 75th and 90th percentiles of the T/L ratios

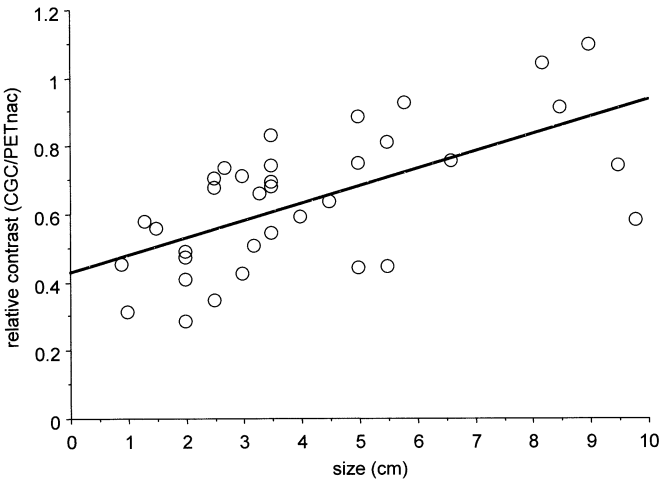

Fig. 5. Tumour/lung ratio of CGC studies relative to PETnac depending on the size of the lesion (n=35, 27 primary tumours and 8 lymph node metastases). There is a statistically significant decrease in the relative contrast of the CGC images with decreasing lesion size (r=0.62, $P<0.01$ by linear regression analysis)

lymph node metastases that were visible in CGC and PETnac studies, the image contrast was 56% lower in CGC than in PETnac. The T/L ratio was 3.7±2.3 (median: 3.2) for CGC and 6.6±3.1 (median: 6.3) for PETnac (P=0.002, Fig. 4). There was a statistically significant decrease in the T/L ratio in the CGC studies relative to the PETnac studies with decreasing lesion size (for pulmonary lesions: r=0.61, P<0.001; all 35 lesions combined: r=0.62, P<0.001 by linear regression analysis). For lesions with a diameter of 0–2 cm, 2–5 cm and more than 5 cm the relative contrast was 0.44±0.11, 0.64±0.14 and 0.81±0.21, respectively (Fig. 5).

Discussion

Dual-head gamma cameras with sodium iodide (NaI) detectors operated in coincidence mode represent a new approach for imaging with positron-labeled tracers. In the present study in lung cancer patients, the CGC visualized all 27 histopathologically proven pulmonary lesions. The lesion to background ratio was approximately 30% lower for the CGC system than for the dedicated ring system. Furthermore, only 8 out of 11 histopathologically proven lymph node metastases were visualized by the CGC system while all 11 metastases were detected by the full-ring system.

Several technical aspects of this study need special consideration. The injected activity (214±49 MBq) was lower than in previous studies using dedicated ring systems for the evaluation of lung cancer patients. In these studies, approximately 370 MBq were administered [5, 20, 21]. The lower injected activity may have introduced a bias against the dedicated PET in comparison with the CGC system. However, all primary tumours and lymph node metastases were detected by the dedicated PET system. The lower activity was necessary to enable early completion of the combined CGC/PET examination. After a dose of 370 MBq, a waiting period of approximately 2 h between the PET and the CGC scan would have been required. This longer waiting period would have complicated the comparison of dedicated PET and CGC scans because of changes in the activity distribution in tumours and normal tissues. To compensate for the lower injected activity, the duration of the emission scan was extended to 20 min, which is longer than in several previous studies using an emission time between 6 and 10 min [20, 21].

An additional technical consideration is that different iterative algorithms were used for the reconstruction of the dedicated PET and CGC studies. The OSEM algorithm is the standard method for image reconstruction with the Vertex MCD camera. Currently, there is no generally available iterative reconstruction package for the ECAT EXACT scanner and filtered backprojection is the standard reconstruction method. In most studies, a Hanning filter with a cut-off frequency of 0.3–0.5 cycles/bin has been applied. Since iterative reconstruction methods have been reported to improve the detectability of lesions compared with filtered backprojection [22], we chose to reconstruct the images iteratively using parameters such that the reconstructed resolution is similar to filtered backprojection with a Hanning filter (cut-off frequency of 0.4 cycles/bin) [23].

Compared with a dedicated ring system, CGC cameras have several technical limitations which impair image quality. The percentage of scattered and random events is considerably higher than for a ring system operated in 2D mode. Phantom studies have shown that the scatter fraction in a cylinder of 20-cm diameter is 32% for the CGC system, whereas it is 17% for the dedicated system used in this study [9, 24]. For a singles count rate of 1.1×10^6/s, the percentage of random coincidences is approximately 25% for a 20-cm cylinder phantom. The corresponding fraction of random events for the dedicated system is only 4% [9, 24]. In patient studies, an even higher percentage of randoms and scattered coincidence can be expected. In addition, pulse pile-up in the detector system limits the singles count rate that can be processed by the CGC system. Both factors result in artefacts and markedly reduce image quality when the singles count rate exceeds 1.5×10^6/s [9]. To overcome this problem, patients were imaged after the singles count rate had dropped below this value. Consequently, the number of coincidence events used for reconstruction per cm axial FOV was 70% lower for the CGC system (trues, scatter, randoms) compared with the dedicated ring system (trues, scatter). Due to decay and excretion of ^{18}F during the interval between the dedicated PET and CGC studies, this number does not directly reflect the physical characteristics of the two camera systems. However, it gives a valid estimate of the relative number of coincidence events that can be acquired in a clinical protocol.

The lower number of coincidence events and the high fraction of scattered and random events explain why, despite comparable spatial resolution, image contrast was significantly lower in the CGC studies than with the dedicated system. Furthermore, the image contrast in the CGC relative to non-attenuation-corrected dedicated PET studies (PETnac) deteriorated significantly with decreasing lesion size. In addition to the high fraction of scattered and random coincidences, this decrease in image contrast may be related to the currently used single slice rebinning method. To increase the number of coincidences for reconstruction, a relatively wide acceptance angle of 15% is used. The resulting axial smearing of the image data may decrease the contrast for small lesions. Furthermore, high uptake in the vicinity of a lesion seems to limit the detectability on CGC images: two lymph nodes with diameters of 1.5 and 2 cm that were located close to the primary tumour were not identified by the CGC camera while they were clearly visible on the PETnac and PETac images (Fig. 3).

In previous studies using dedicated PET systems, FDG imaging has been very successful in the differenti-

ation of benign and malignant pulmonary nodules and mediastinal staging of lung cancer. Is there currently a role for CGC systems in these clinical applications? In the evaluation of lymph node metastases, metabolic imaging using FDG has two principal advantages over CT: On the one hand, focal FDG accumulation may allow the detection of metastatic deposits in lymph nodes that are not yet enlarged. On the other hand, non-specifically enlarged lymph nodes without tumour involvement generally show no increase in FDG uptake. Due to these two advantages, the sensitivity and specificity of dedicated PET systems in the evaluation of lymph node involvement have been consistently found to be superior to those of CT [5, 6, 25]. In the present study, 3 out of 11 lymph node metastases that were detected by the dedicated PET system were not visualized by CGC imaging. Furthermore, as indicated above, the image contrast in CGC studies relative to the dedicated system deteriorated significantly with decreasing lesion size. For lesions with a diameter of 1 cm, the image contrast was approximately 60% lower than with the dedicated PET system. Therefore, visualization of lymph node metastases with a diameter of less than 1 cm is only possible for metabolically highly active lesions. In CT studies, a lymph node diameter of more than 1 cm is generally used as a criterion for tumour involvement. Therefore, CGC systems will probably not provide an increased sensitivity compared with CT in the evaluation of mediastinal lymph node metastases. However, the specificity of CGC appears to be comparable to that of dedicated PET systems. Both imaging methods were true negative in 75 of 77 surgically sampled lymph node stations. In contrast, false-positive CT results occurred in six lymph node stations. Therefore, CGC studies may provide complementary information to CT in the mediastinal staging of lung cancer. For example, in patients with advanced disease who are candidates for primary radiotherapy or neo-adjuvant therapeutic regimens, CGC imaging studies may be helpful in the evaluation of lymph nodes that are not accessible by mediastinoscopy.

The CGC results regarding the evaluation of pulmonary nodules are more encouraging. All primary tumours were detected with a mean tumour to lung ratio of 4.7. However, detection was facilitated by the size of the lesions: 24 of the 27 lesions had a diameter of 2 or more cm and the mean diameter was 4.6 cm. Furthermore, the FDG uptake of the tumour tissue was high, with a mean SUV of 6.9. Additionally, the study population was highly selected since all patients had a strong clinical suspicion for a malignant lung tumour or biopsy-proven lung cancer. Consequently, the findings of the present study cannot be directly extrapolated to an evaluation of indeterminate solitary pulmonary nodules. Nevertheless, the high contrast of the pulmonary lesions suggests that CGC imaging provides a similar sensitivity to a full-ring PET system in the detection of malignant pulmonary nodules with a diameter of 2 cm or more. In previous clinical studies evaluating indeterminate solitary pulmonary nodules with FDG and dedicated PET systems, the mean size of the lesions ranged between 1.8 and 3 cm [2, 26–28]. In a recently published study that included only pulmonary nodules with diameters of 3 cm or less, 36% of the nodules had a diameter of 2 cm or more [28]. Even when applying a size limit of 2 cm, coincidence imaging may be a useful test in a relatively large percentage of patients presenting with indeterminate pulmonary nodules.

In the future, the sensitivity of CGC imaging for small lesions may be improved by the use of attenuation correction. New methods to acquire transmission measurements for attenuation correction have recently been introduced but have not yet been validated in clinical trials [29]. Currently, there is controversy over the effect of attenuation correction on lesion detectability in oncological FDG-PET studies. Improved visualization of small and deep-seated lesions has been reported in some cases [30]; however, a consistent improvement in diagnostic accuracy has not yet been documented [31, 32]. In the present study, one mediastinal lymph node with a diameter of 0.75 cm was only detected on the attenuation-corrected dedicated PET images. For staging of lung cancer, the transmission images provide very helpful anatomical landmarks, such as the trachea and the main bronchi. Therefore, the localization of focal FDG uptake in the mediastinum is greatly facilitated. This is important for subsequent histopathological verification of abnormal findings in CGC studies by mediastinoscopy or biopsy.

In conclusion, this initial evaluation of dual-head gamma camera coincidence imaging in lung cancer yielded encouraging results. Detectability of pulmonary lesions with a diameter of at least 2 cm appears to be similar to a dedicated ring system. The sensitivity of coincidence imaging for detection of small lymph node metastases is limited by a lower image contrast which deteriorates relative to the dedicated system with decreasing lesion size. However, the specificity for the evaluation of lymph node involvement is comparable between the two systems. It is expected that improved imaging technology of coincidence cameras and commercially supported distribution of FDG will have a major impact on the development of more widely available and less costly metabolic imaging in patients with oncological diseases.

Acknowledgements. We gratefully acknowledge the efforts of the cyclotron and radiochemistry staff. Furthermore, we appreciate the excellent technical support by the technologists at our institution. We thank J. Fessler, PhD, University of Michigan, for generously providing the software for the iterative reconstruction of the dedicated PET studies. This study was financially supported by ADAC Laboratories, Milpitas, Calif.

References

1. Rigo P, Paulus P, Kaschten BJ, Hustinx R, Bury T, Jerusalem G, Benoit T, Foidart WJ. Oncological applications of positron emission tomography with fluorine-18 fluorodeoxyglucose. *Eur J Nucl Med* 1996; 23: 1641–1674.
2. Kubota K, Matsuzawa T, Fujiwara T, Ito M, Hatazawa J, Ishiwata K, Iwata R, Ido T. Differential diagnosis of lung tumour with positron emission tomography: a prospective study. *J Nucl Med* 1990; 31: 1927–1932.
3. Patz EF, Lowe VJ, Hoffman JM, Paine SS, Burrowes P, Coleman RE, Goodman PC. Focal pulmonary abnormalities: evaluation with F-18 fluorodeoxyglucose PET scanning. *Radiology* 1993; 188: 487–490.
4. Gupta NC, Maloof J, Gunel E. Probability of malignancy in solitary pulmonary nodules using fluorine-18-FDG and PET. *J Nucl Med* 1996; 37: 943–948.
5. Wahl RL, Quint LE, Greenough RL, Meyer CR, White RI, Orringer MB. Staging of mediastinal non-small cell lung cancer with FDG PET, CT, and fusion images: preliminary prospective evaluation. *Radiology* 1994; 191: 371–377.
6. Steinert HC, Hauser M, Allemann F, Engel H, Berthold T, von Schulthess GK, Weder W. Non-small cell lung cancer: nodal staging with FDG PET versus CT with correlative lymph node mapping and sampling. *Radiology* 1997; 202: 441–446.
7. Scott WJ, Schwabe JL, Gupta NC, Dewan NA, Reeb SD, Sugimoto JT. Positron emission tomography of lung tumours and mediastinal lymph nodes using [^{18}F]fluorodeoxyglucose. The Members of the PET-Lung Tumor Study Group. *Ann Thorac Surg* 1994; 58: 698–703.
8. Lowe VJ, Fletcher JW, Gobar L, Lawson M, Kirchner P, Valk P, Karis J, Hubner K, Delbeke D, Heiberg EV, Patz EF, Coleman RE. Prospective investigation of positron emission tomography in lung nodules. *J Clin Oncol* 1998; 16: 1075–1084.
9. Ziegler SI, Enterrottacher A, Boning G, Schwaiger M. Performance characteristics of a dual head coincidence camera for the detection of small lesions [abstract]. *J Nucl Med* 1997; 38: 206.
10. Shreve P, Steventon R, Deters E, Kison P, Gross M, Wahl M. Oncological diagnosis with 2-[fluorine-18]fluoro-2-deoxy-D-glucose imaging: dual head coincidence gamma camera versus positron emission tomographic scanner. *Radiology* 1998; 207: 431–437.
11. Hamacher K, Coenen HH, Stocklin G. Efficient stereospecific synthesis of no-carrier-added 2-[^{18}F]-fluoro-2-deoxy-D-glucose using aminopolyether supported nucleophilic substitution. *J Nucl Med* 1986; 27: 235–238.
12. Wienhard K, Dahlbom M, Eriksson L, Michel C, Bruckbauer T, Pietrzyk U, Heiss WD. The ECAT EXACT HR: performance of a new high resolution positron scanner. *J Comput Assist Tomogr* 1994; 18: 110–118.
13. Fessler J. Penalized weighted least-squares image reconstruction for positron emission tomography. *IEEE Trans Med Imaging* 1994; 13: 290–300.
14. Hudson H, Larkin R. Accelerated image reconstructiion using ordered subsets of projection data. *IEEE Trans Med Imaging* 1994; 13: 601–609.
15. Mountain C. Revisions of the international system for staging lung cancer. *Chest* 1997; 111: 1710–1717.
16. McLoud T, Bourgouin P, Grenberg R, Kosiuk J, Templeton P, Shepard J-A, Moore E, Wain J, Mathisen D, Grillo H. Bronchogenic carcinoma: analysis of staging in the mediastinum with CT by correlative lymph node mapping and sampling. *Radiology* 1992; 182: 319–323.
17. Lewis J, Pearlberg J, Beute G, Alpern M, Kvale P, Gross B, Magilligan D. Can computed tomography of the chest stage lung cancer? - Yes and no. *Ann Thorac Surg* 1990; 49: 591–596.
18. Kiyono K, Sone S, Sakai F, Ima Y, Watanabe T, Izuno I, Oguchi M, Kawai T, Shitematsu H, Watanabe M. The number and size of normal mediastinal lymph nodes: a postmortem study. *AJR Am J Roentgenol* 1988; 150: 771–776.
19. Strauss LG, Conti PS. The applications of PET in clinical oncology. *J Nucl Med* 1991; 32: 623–648; discussion 649–650.
20. Scott WJ, Gobar LS, Terry JD, Dewan NA, Sunderland JJ. Mediastinal lymph node staging of non-small-cell lung cancer: a prospective comparison of computed tomography and positron emission tomography. *J Thorac Cardiovasc Surg* 1996; 111: 642–648.
21. Sazon DA, Santiago SM, Soo HGW, Khonsary A, Brown C, Mandelkern M, Blahd W, Williams AJ. Fluorodeoxyglucose-positron emission tomography in the detection and staging of lung cancer. *Am J Respir Crit Care Med* 1996; 153: 417–421.
22. Llacer J, Veklerov E, Baxter LR, Grafton ST, Griffeth LK, Hawkins RA, Hoh CK, Mazziotta JC, Hoffman EJ, Metz CE. Results of a clinical receiver operating characteristic study comparing filtered backprojection and maximum likelihood estimator images in FDG PET studies. *J Nucl Med* 1993; 34: 1198–1203.
23. Becker S, Ziegler S, Weber W, Römer W, Avril N, Schwaiger M. Iterative reconstruction of FDG-PET data: diagnostic value compared to filtered backprojection. *J Nucl Med* 1997; 101P.
24. Wienhard K, Eriksson L, Grootoonk S, Casey M, Pietrzyk U, Heiss WD. Performance evaluation of the positron scanner ECAT EXACT. *J Comput Assist Tomogr* 1992; 16: 804–813.
25. Vansteenkiste JF, Stroobants SG, De Leyn PR, Dupont PJ, Bogaert J, Maes A, Deneffe GJ, Nackaerts KL, Verschakelen JA, Lerut TE, Mortelmans LA, Demedts MG. Lymph node staging in non-small-cell lung cancer with FDG-PET scan: a prospective study on 690 lymph node stations from 68 patients. *J Clin Oncol* 1998; 16: 2142–2149.
26. Dewan NA, Gupta NC, Redepenning LS, Phalen JJ, Frick MP. Diagnostic efficacy of PET-FDG imaging in solitary pulmonary nodules. Potential role in evaluation and management. *Chest* 1993; 104: 997–1002.
27. Lowe VJ, Hoffman JM, DeLong DM, Patz EF, Coleman RE. Semiquantitative and visual analysis of FDG-PET images in pulmonary abnormalities. *J Nucl Med* 1994; 35: 1771–1776.
28. Praeuer HW, Weber WA, Roemer W, Treumann T, Ziegler SI, Schwaiger M. Controlled prospective study of positron emission tomography using the glucose analogue F-18-fluorodeoxyglucose in the evaluation of pulmonary nodules. *Br J Surg* 1998; 85: 1506–1511.
29. Shao L, Nelleman P, Muehllehner G, Bertelsen H, Hines H. Singles-transmission attenuation correction for dual head coincidence imaging. *J Nucl Med* 1998; 37: 37P.
30. Bedigian M, Benard F, Smith R, Karp J, Alavi A. Whole-body positron emission tomography for oncology imaging using singles transmission scanning with segmentation and ordered sub-sets-expectation maximization (OS-EM) reconstruction. *Eur J Nucl Med* 1998; 25: 659–661.
31. Bengel FM, Ziegler SI, Avril N, Weber W, Laubenbacher C, Schwaiger M. Whole-body positron emission tomography in clinical oncology: comparison between attenuation-corrected and uncorrected images. *Eur J Nucl Med* 1997; 24: 1091–1098.
32. Imran B, Kubota K, Yamada S, Fukuda H, Ymada K, Fujiwara T, Itoh M. Lesion-to-background ratio in nonattenuation-corrected whole-body FDG PET images. *J Nucl Med* 1998; 39: 1219–1223.